OPINCHARGE

OPINCHARGE

D5.2 Charge transport characteristics – Correlation of structure, chemistry and charge transport and their dynamics

5/2026

Funded by
the European Union

Lead Beneficiary	**Forschungszentrum Jülich GmbH (FZJ)**
Author(s)/Organisation(s)	**Xiaokun Ge, Hans-Georg Steinrück**
Contact Email	**x.ge@fz-juelich.de; h.steinrueck@fz-juelich.de**
Contributor(s)	**German Aerospace Center (DLR), Lukas Köbing, Birger Horstmann**
Work Package	**WP5, Task 5.3 Correlation of interface structure and chemistry with electronic and ionic transport mechanisms and rates**
Delivery Date (DoA)	**31/05/2026**
Actual Delivery Date	**19/05/2026**
Abstract:	The influence of the solid electrolyte interphase (SEI) on interfacial electron and ion transfer remains difficult to assess directly. Here, the ferrocene/ferrocenium (Fc/Fc^+) couple was used as a redox probe to study electron and ion transfer across a pre-formed LiF-based model SEI (LiF-SEI) on planar Au and Pt electrodes. Reference measurements on pristine electrodes showed stable and reproducible Fc/Fc^+ redox behaviour. After LiF-SEI formation, the Fc response differed strongly between the two substrates. On Pt, the redox current density was initially suppressed but recovered progressively during repeated cycling. On Au, the redox response remained strongly suppressed and no clearly defined redox peak pair developed. Electrochemical measurements, Scanning Electron Microscopy (SEM), and Electrochemical Quartz Crystal Microbalance with Dissipation (EQCM-D) further showed clear differences in interphase formation on Au and Pt. Au exhibited a more homogeneous and compact interphase, whereas Pt showed more heterogeneous and mechanically complex behaviour. Different evaluation methods consistently indicated a thicker interphase on Pt than on Au.

Document Revision History			
Date	**Version**	**Author/Contributor/Reviewer**	**Summary of Main Changes**
22/04/2026	v0.1	Xiaokun Ge	Creation
06/05/2026	v0.2	Lukas Köbbing (DLR)	Simulation Parts
06/05/2026	v0.3	Hans-Georg Steinrück	Editing
17/05/2026	v1.0	Xiaokun Ge	Editing
18/05/2026	v1.1	Hans-Georg Steinrück	Editing
19/05/2026	v2.0	Xiaokun Ge	Finalization

Dissemination Level and Nature of the Deliverable		
PU	Public	Yes
Nature	R = Report, E = Ethics or, O = Other	R

OPINCHARGE Consortium			
#	Participant Organisation Name	Short Name	Country
1	LUXEMBOURG INSTITUTE OF SCIENCE AND TECHNOLOGY (LIST)	LIST	LU
2	CENTRE NATIONAL DE LA RECHERCHE SCIENTIFIQUE CNRS (CNRS)	CNRS	FR
3	CENTRO DE INVESTIGACION COOPERATIVA DE ENERGIAS ALTERNATIVAS FUNDACION, CIC ENERGIGUNE FUNDAZIOA (CIC ENERGIGUNE)	CIC ENERGIGUNE	ES
4	DEUTSCHES ZENTRUM FUR LUFT - UND RAUMFAHRT EV (DLR)	DLR	DE
5	DEUTSCHES FORSCHUNGSZENTRUM FUR KUNSTLICHE INTELLIGENZ GMBH (DFKI)	DFKI	DE
6	FEI ELECTRON OPTICS BV (THERMO)	THERMO	NL
7	FUNDACION CIDETEC (CIDETEC)	CIDETEC	ES
8	FORSCHUNGSZENTRUM JÜLICH (FZJ)	FZJ	DE
9	PEDAL CONSULTING SRO (PEDAL)	PEDAL	SK
10	PAUL SCHERRER INSTITUT (PSI)	PSI	CH

NOTICE

Funded by the European Union under grant agreement number 101104032 . Views and opinions expressed are however those of the author(s) only and do not necessarily reflect those of the European Union or European Climate, Infrastructure and Environment Executive Agency (CINEA). Neither the European Union nor the granting authority can be held responsible for them.

OPINCHARGE

Grant Agreement: 101104032 .

Call: HORIZON-CL5-2022-D2-01.

Topic: HORIZON-CL5-2022-D2-01-02.

Type of action: HORIZON Research and Innovation Actions.

Granting authority: European Climate, Infrastructure and Environment Executive Agency.

Grant managed through EU Funding & Tenders Portal: Yes (eGrants).

Project starting date: fixed date: 1 June 2023.

Project end date: 31 May 2026.

Project duration: 36 months.

Table of Contents

List of Figures

List of Abbreviations and Acronyms	
SEI	Solid Electrolyte Interphase
LIBs	Lithium-ion Batteries
Fc	Ferrocene
Fc^+	Ferrocenium
WE	Working Electrode
CE	Counter Electrode
RE	Reference Electrode
EQCM-D	Electrochemical Quartz Crystal Microbalance with Dissipation
LiF-SEI	LiF-based model SEI
OCV	Open-circuit Voltage
LSV	Linear Sweep Voltammetry
CA	Chronoamperometry
CV	Cyclic Voltammetry
LP40	1 M $LiPF_6$ in EC/DEC = 50/50 (v/v)
SEM	Scanning Electron Microscopy
XPS	X-ray Photoelectron Spectroscopy

1 Introduction

The solid electrolyte interphase (SEI) is essential for the stabilization of negative electrodes in lithium-ion batteries (LIBs), as it suppresses continuous electrolyte decomposition and thereby enables long-term electrochemical operation. In general, the SEI is a thin interphase layer composed of electrolyte decomposition products and contains both organic and inorganic species. It is commonly described as a multilayer structure with a more porous and heterogeneous organic outer region and a denser inorganic inner region close to the electrode surface (as schematically shown in Figure 1). [1] Among the inorganic SEI components, LiF is often considered particularly important because a dense and homogeneous LiF-rich layer can effectively isolate the electrode from the electrolyte while still allowing Li-ion transport. At the same time, the quality of the SEI remains difficult to assess directly, since its formation, chemistry, structure, and transport properties strongly depend on the electrolyte and the electrode surface. Because the SEI controls the extent to which further parasitic electrolyte reduction is suppressed, experimental approaches are needed that allow its effect on interfacial electron transfer to be probed in a direct and quantitative manner. [2]

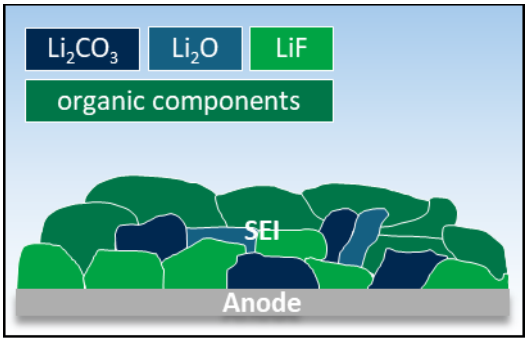

Figure 1 Schematic illustration of the multilayer structure of the SEI formed on the negative electrode surface.

This question is closely connected to the objectives of Work Package 5 (WP5), *Interface Modelling and Validation Using Experimental Charge Transport Characteristics*. Within WP5, Task 5.3 addresses how the structure and chemistry of the SEI affect electronic and ionic transport across the interface. The work presented here focuses on the electronic part of this task. For this purpose, the ferrocene/ferrocenium (Fc/Fc^+) redox couple is used as an electrochemical probe to study electron transfer across pre-formed SEI layers. To study this under controlled conditions, planar Au and Pt electrodes were used as model substrates. In contrast to composite electrodes, flat metal electrodes minimize additional complexity arising from cracking, large morphology changes, or heterogeneous porous electrode structures. This makes it possible to examine more directly how SEI formation affects the electrochemical response of Fc/Fc^+ and, consequently, interfacial electron transfer. The present contribution therefore provides an experimental basis for relating SEI formation and passivation behavior to electron transport at the electrode/SEI/electrolyte interface.

2 Experimental Methodology

2.1 Concept of the Fc/Fc⁺ redox probe for electron transport

The basic idea of the present approach is to probe how the SEI affects electron transfer at the electrode/electrolyte interface by comparing the electrochemical response of a dissolved redox couple before and after SEI formation. As illustrated in Figure 2, a reference voltammogram of the Fc/Fc⁺ redox couple is first recorded on a pristine planar metal electrode. After formation of the SEI on the same type of electrode surface, the Fc/Fc⁺ response is measured again under comparable conditions. The difference between the reference response and the response obtained after SEI formation is then used to assess how the SEI modifies interfacial electron transfer. For this purpose, not only the current density, but also the peak positions and the overall shape of the voltammograms are considered.

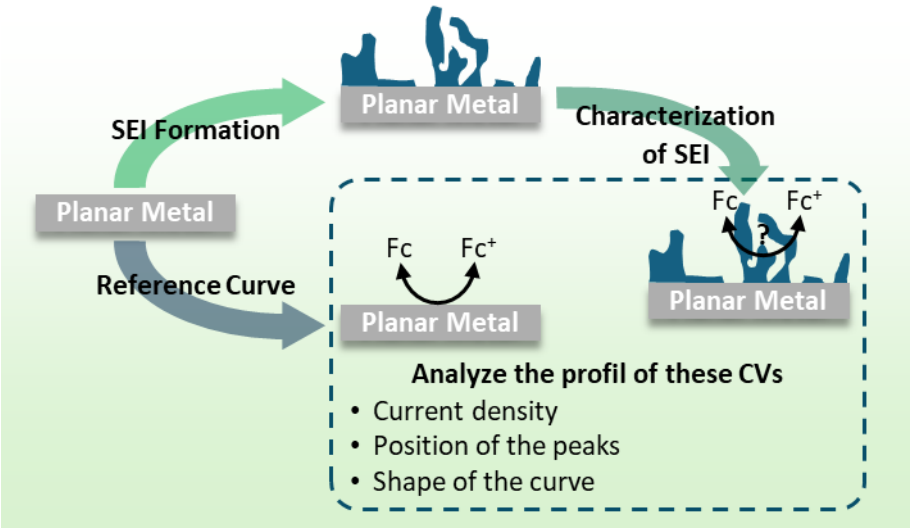

Figure 2 Schematic representation of the experimental concept used to probe electron transfer across the SEI by comparing the Fc/Fc⁺ voltammetric response before and after SEI formation on planar metal electrodes.

Fc is particularly suitable as a redox probe in non-aqueous electrolytes because of its good solubility, chemical stability, and well-defined electrochemical reversibility. In addition, the Fc/Fc⁺ redox couple undergoes an outer-sphere electron-transfer reaction, making it especially useful for probing changes in electron transfer at the interface without requiring a specific chemical interaction with the surface.[3]

Depending on the properties of the SEI, different changes in the Fc/Fc⁺ response can be expected, as schematically illustrated in Figure 3. In the absence of an SEI (a), the voltammetric response reflects electron transfer at the clean electrode surface. If the SEI is thin enough (c) that electron tunneling still contributes to charge transfer, the electron-transfer kinetics may be modified, which can appear as peak shifts and changes in peak separation. [4] In the case of a porous SEI (d), where electron transfer takes place only at localized sites or through pore-mediated pathways, the voltammetric response may evolve towards a S-shape. [5] For a more strongly blocking SEI (b), the Fc/Fc⁺ response can be significantly suppressed. The combined analysis of current response, peak position, and curve shape therefore provides the basis for evaluating how the SEI influences electron transfer across the electrode/SEI/electrolyte interface.

In addition to the Fc/Fc^+ redox response, complementary electrochemical quartz crystal microbalance with dissipation (EQCM-D) measurements were carried out in order to monitor interfacial changes during LiF-SEI formation and during subsequent Fc probing. While the Fc/Fc^+ method is sensitive to changes in electron-transfer behaviour across the SEI, it does not directly distinguish between possible contributions such as variations in interphase mass, structural evolution, or changes in the mechanical properties of the interphase. EQCM-D was therefore used as a complementary tool to provide additional insight into these processes.

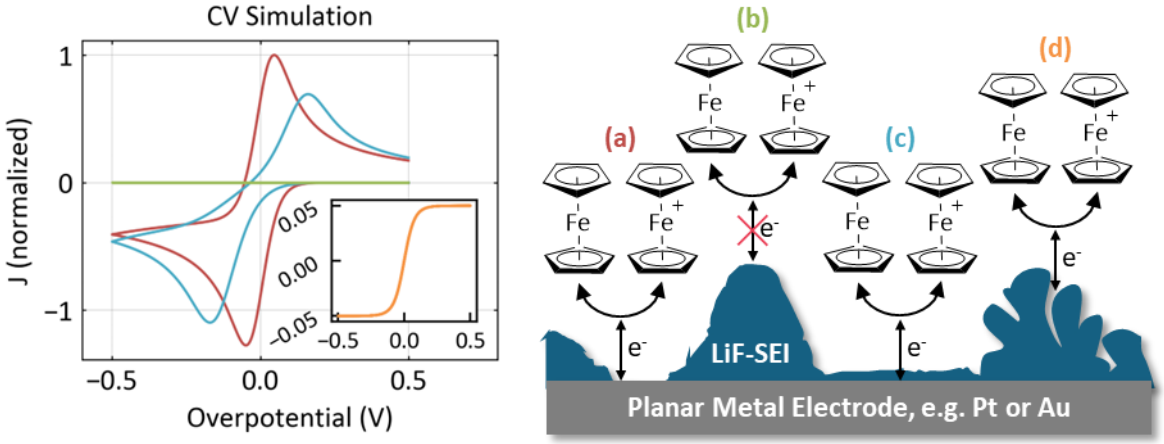

Figure 3 Simulated Fc/Fc^+ voltammetric responses for different interfacial situations and schematic illustration of the corresponding SEI-covered planar metal electrode. Depending on SEI coverage and electron-transfer limitations, changes in current, peak position, and voltammetric shape can occur.

2.2 Cell configuration and experimental setup

To realize the idea described above, a modified PEEK cone-type electrochemical cell was used, as schematically shown in Figure 4. The detailed design of this cell was reported previously.[6] For sealing, a PMMA base and a stainless-steel lid were used and fixed together by four screws. The cell contains a conventional wafer-type working electrode (WE), either Pt-coated Si or Au-coated Si, providing a planar metal surface. Lithium metal was used as both counter electrode (CE) and reference electrode (RE). Unless stated otherwise, all electrolytes used in this work were pre-saturated with LiF to minimize dissolution of LiF from the SEI. In the following, this is not stated explicitly for each electrolyte composition.

For EQCM/D measurements a commercial Li research in-batch cell (AWSensors) was used to mount standard AT-cut 5 MHz quartz crystal sensors with polished Au electrodes (AWSensors).

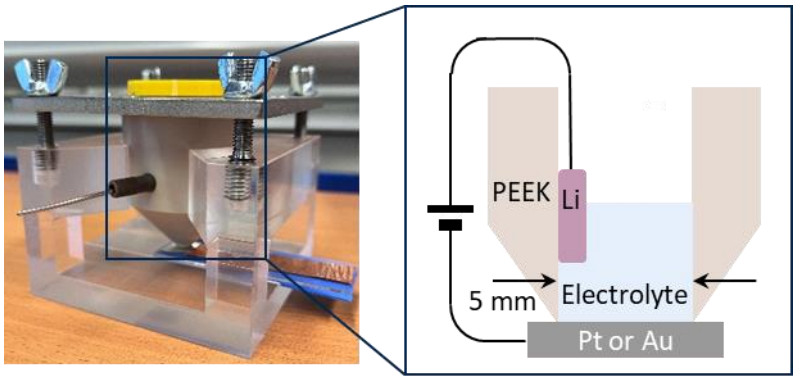

Figure 4 Photograph of the modified PEEK cone-type electrochemical cell used in this work, together with a schematic illustration of its internal configuration.

2.3 Electrochemical measurement protocol

Before describing the experimental steps, we briefly explain the choice of the model interphase used in this work. To simplify the complexity of the SEI, a LiF-based model SEI (denoted as “LiF-SEI”) was used. LiF is a key inorganic component of the inner SEI and is electronically insulating. In this work, it was generated by potential-controlled electrocatalytic reduction of HF (Equation 1). [7]

$$HF + Li^+ + e^- \rightarrow LiF + H_{ad} \quad (1)$$

The electrochemical workflow used in this work is summarized in Figure 5. The standard protocol consisted of two main steps: formation of the LiF-SEI on planar electrodes, followed by probing of the formed LiF-SEI with the Fc/Fc^+ redox couple. For LiF-SEI formation, the cell was filled with 0.5 mL of LP40 (1 M $LiPF_6$ in EC/DEC = 50/50 (v/v)). After recording the open-circuit voltage (OCV) for 15 min, linear sweep voltammetry (LSV) was performed from OCV to 1.7 V vs. Li/Li^+ at 1 mV/s, followed by chronoamperometry (CA) at 1.7 V vs. Li/Li^+ for 3 h (or more). The lower potential limit of 1.7 V vs. Li/Li^+ was chosen to promote HF reduction and thus LiF formation, while avoiding the lower-potential regime in which additional electrolyte reduction processes become significant. For the Fc/Fc^+ measurements, reference voltammograms were first recorded. Cyclic voltammetry (CV) was carried out between 2.7 and 3.6 V vs. Li/Li^+ at 20 mV/s for 20 cycles in a 1:1 (v/v) mixture of LP40 and 6.6 mM Fc solution. After SEI formation, 0.5 mL of the Fc solution was added to the cell, mixed thoroughly, and the Fc/Fc^+ response was measured again under the same basic CV conditions. This allowed direct comparison of the voltammetric response before and after LiF-SEI formation.

The parameters shown in Figure 5 represent the basic procedure used throughout this study. In selected experiments, systematic variations were introduced to test specific hypotheses, while the overall workflow remained unchanged. Unless stated otherwise, these experiments were performed in triplicate, and all experiments were carried out on both Pt and Au. The EQCM-D measurements followed the same general workflow.

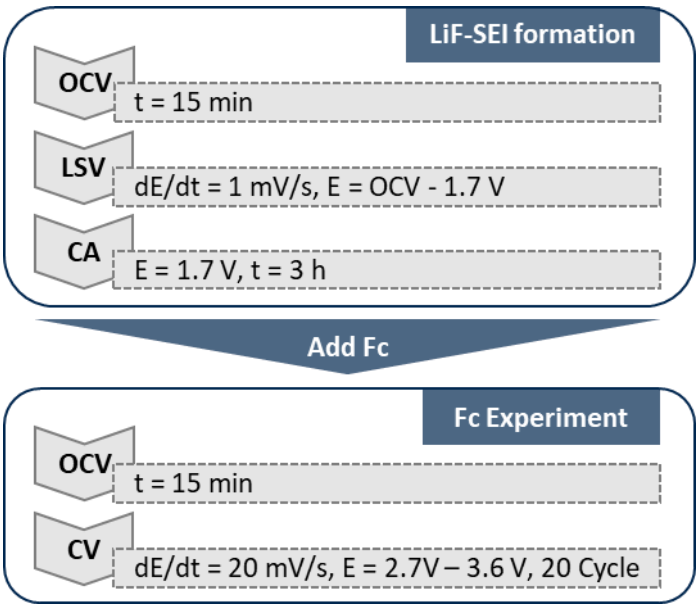

Figure 5 Electrochemical protocol used in this work for LiF-SEI formation and subsequent Fc/Fc^+ probing, including the main electrochemical techniques and the standard parameters of the basic measurement sequence.

2.4 Simulation

To interpret the experimental results, we perform simulations of the cyclic voltammetry procedure. For the basic simulation setup, we consider the current density j of the redox reaction by the Butler-Volmer equation

$$j = j_0 \left(c_O \exp\left(-\frac{\alpha F \eta}{RT}\right) - c_R \exp\left(\frac{\alpha F \eta}{RT}\right)\right)$$

with the exchange current density j_0, the surface concentrations of the oxidized c_O and the reduced species c_R, the charge transfer coefficient $\alpha = 0.5$, the Faraday constant F, the overpotential η, the universal gas constant R, and the temperature T.

Moreover, we assume planar diffusion of the oxidized and reduced species c_i according to Fick's second law

$$\frac{\partial c_i}{\partial t} = D_i \frac{\partial^2 c_i}{\partial x^2}$$

with the time t and the distance from the electrode x.

We extend this basic setup by considering tunneling through the SEI and the influence of a porous SEI layer on the cyclic voltammogram. The results of our simulations are discussed in Section 3.43.4.Simulation

3 Results and Discussion

3.1 Reference response of Fc/Fc$^+$ at a pristine electrode

Before LiF-SEI formation, the Fc/Fc$^+$ response was measured on Au and Pt to establish the reference behavior of the redox probe. Under the chosen conditions, the cyclic voltammograms recorded at 20 mV/s showed a highly consistent response over 20 cycles on both metal surfaces. The voltammograms exhibited a well-defined redox peak pair, indicating good stability and reproducibility of the Fc/Fc$^+$ signal. This reference response was used as the baseline for evaluating the changes observed after LiF-SEI formation.

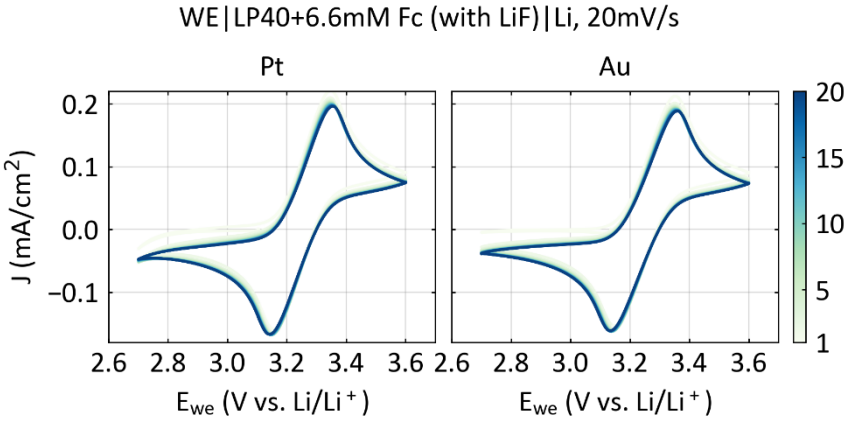

Figure 6 Cyclic voltammograms of the Fc reference measurement recorded between 2.7 and 3.6 V vs. Li/Li$^+$ at a scan rate of 20 mV/s for 20 cycles. The left panel shows the response on Pt, and the right panel shows the response on Au.

3.2 Electrochemical formation of the LiF-SEI

The duration of LiF-SEI formation was controlled by adjusting the chronoamperometric holding time. It was found that extending the formation time up to 70 h did not lead to major differences in the total charge passed, compared with the interphase formed within 3 h. On this basis, all subsequent experiments were carried out using a formation time of 3 h. Figure 7 shows the current response recorded during LiF-SEI formation on Pt (upper panel) and Au (lower panel) as a function of time. The corresponding insets show the LSV curves recorded during the formation process. Several clear differences between the two metal substrates can be observed. (1) The electrocatalytic HF reduction peak appears at higher overpotential on Pt than on Au [7], and the maximum peak current density is also higher on Pt. (2) In addition to the HF reduction peak, Pt shows a further reduction feature at around 1.8 V vs. Li/Li^+, which contributes significantly to the cumulative charge passed during the formation step. In contrast, for Au no additional reduction peak is observed after the HF reduction, and the current decreases to values close to zero. (3) Another noticeable difference concerns the reproducibility of parallel measurements. The three parallel Pt samples show a variation in the current response and peak position than the corresponding Au samples, indicating lower reproducibility of the formation behavior on Pt under the chosen conditions – the reason for this is currently under investigation. Overall, although the same electrochemical protocol was applied to both substrates, the formation behavior differs between Pt and Au, both in terms of the reduction features observed and the overall electrochemical response during the formation step. To further examine whether these differences are also reflected in the interphase growth behavior, complementary *in-situ* EQCM-D measurements were carried out.

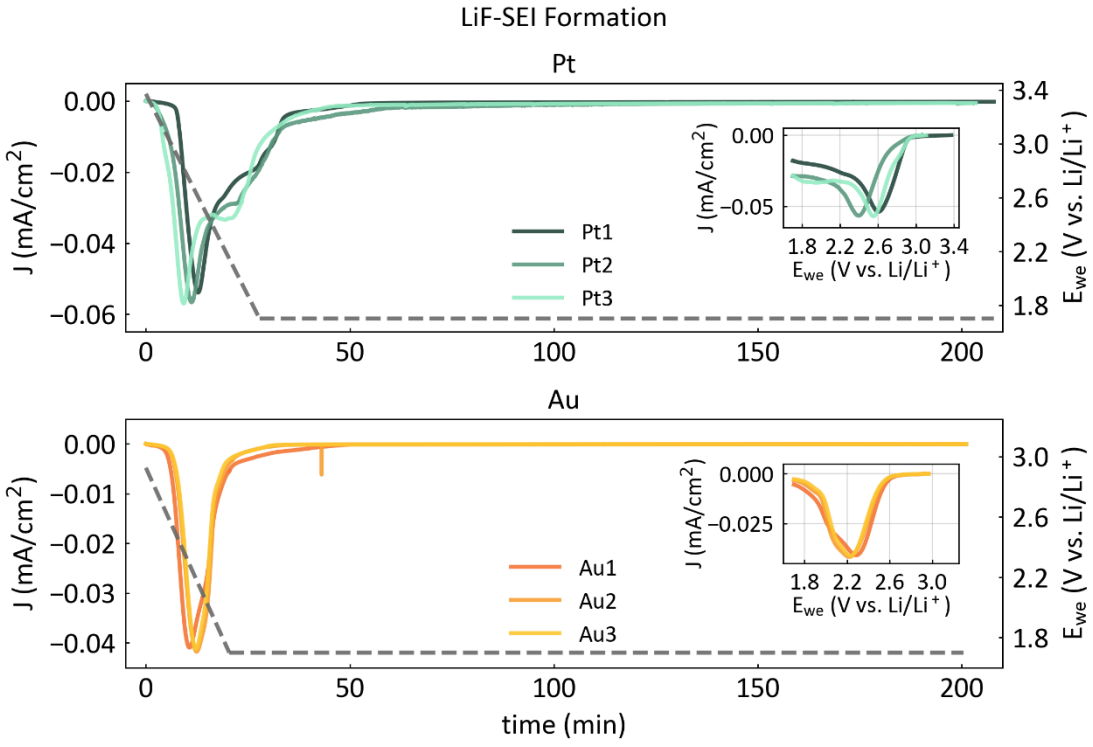

Figure 7 Time-dependent potential and current responses during the electrochemical formation of the LiF-SEI. The upper panel presents the three parallel Pt samples, and the lower panel presents the three parallel Au samples. Inset: Current - voltage curve recorded during the LSV.

Figure 8 and Figure 9 show the normalized frequency shifts ($\Delta f/n$) and dissipation shifts (ΔD) recorded at different overtones during LiF-SEI formation on Pt and Au, respectively. For both substrates, the

EQCM-D response was closely correlated with the electrochemical current response. In the potential region where the current density decreased sharply, corresponding to the HF reduction peak, pronounced changes in both *Δf/n* and *ΔD* were observed, indicating that significant interfacial changes accompanied the electrochemical formation step. For Pt, the EQCM-D response showed a pronounced separation between the different overtones. The difference in normalized frequency shift between the fundamental frequency and the highest overtone reached approximately 1200 Hz. The dissipation shift was also large, reaching values of around 400 × 10^{-6} at the fundamental frequency and the dissipation response differed clearly between the individual overtones. Another noticeable feature is that the evolution of *Δf/n* during the LSV step does not follow a single constant slope but rather exhibits two distinct slope regimes. This suggests that the interphase evolution on Pt does not proceed in a simple single-step manner but instead involves at least two stages with different rates or dominant interfacial processes. Together with the large dissipation response and the strong overtone dispersion, these observations indicate that the interphase formed on Pt is not a thin rigid LiF layer, but rather a more complex and highly viscoelastic interfacial layer, likely containing a substantial liquid-coupled contribution. In contrast, the EQCM-D results obtained on Au were rather similar across the different overtones. The difference in normalized frequency shift between the fundamental frequency and the highest overtone was only about 200 Hz, and the dissipation shifts were also markedly smaller, with relatively little variation between the different overtones. Overall, this behavior suggests that the interphase formed on Au is mechanically more compact and less viscoelastic than that formed on Pt. In other words, the LiF-SEI formed on Au appears to be comparatively denser and more rigid.

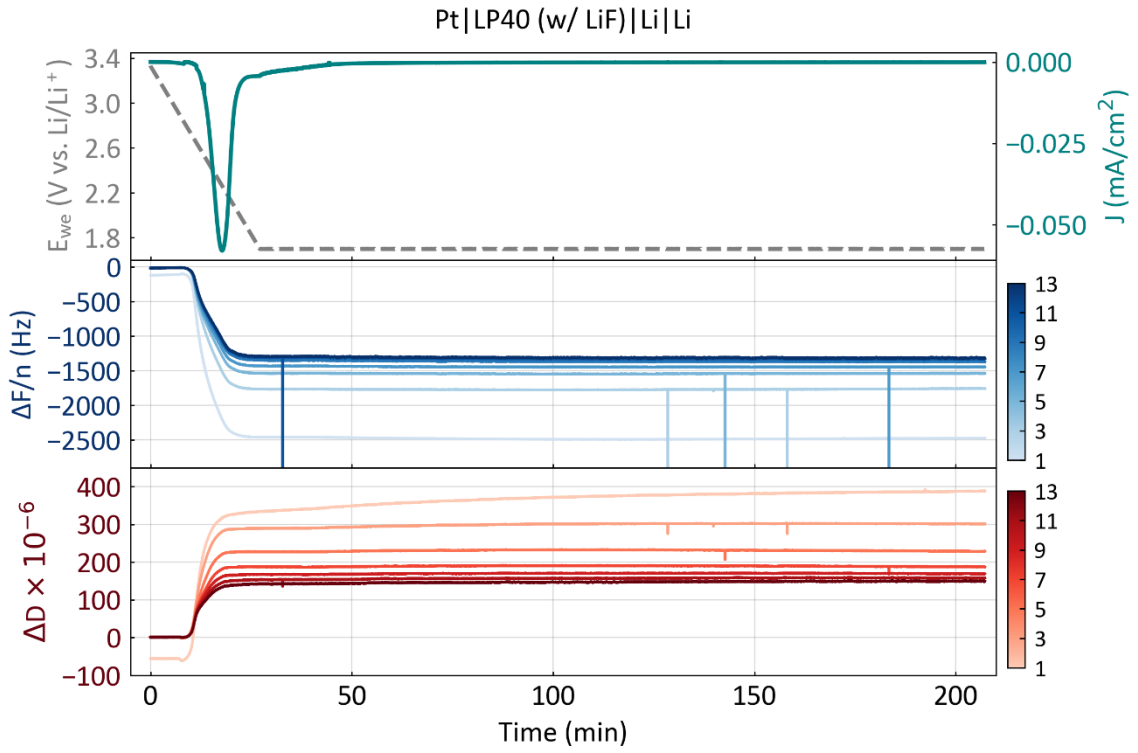

Figure 8 EQCM-D response during LiF-SEI formation on Pt. From top to bottom: time-dependent working electrode potential (left) and current density (right); normalized frequency shifts (ΔF/n) for different overtones; and dissipation shifts (ΔD) for different overtones.

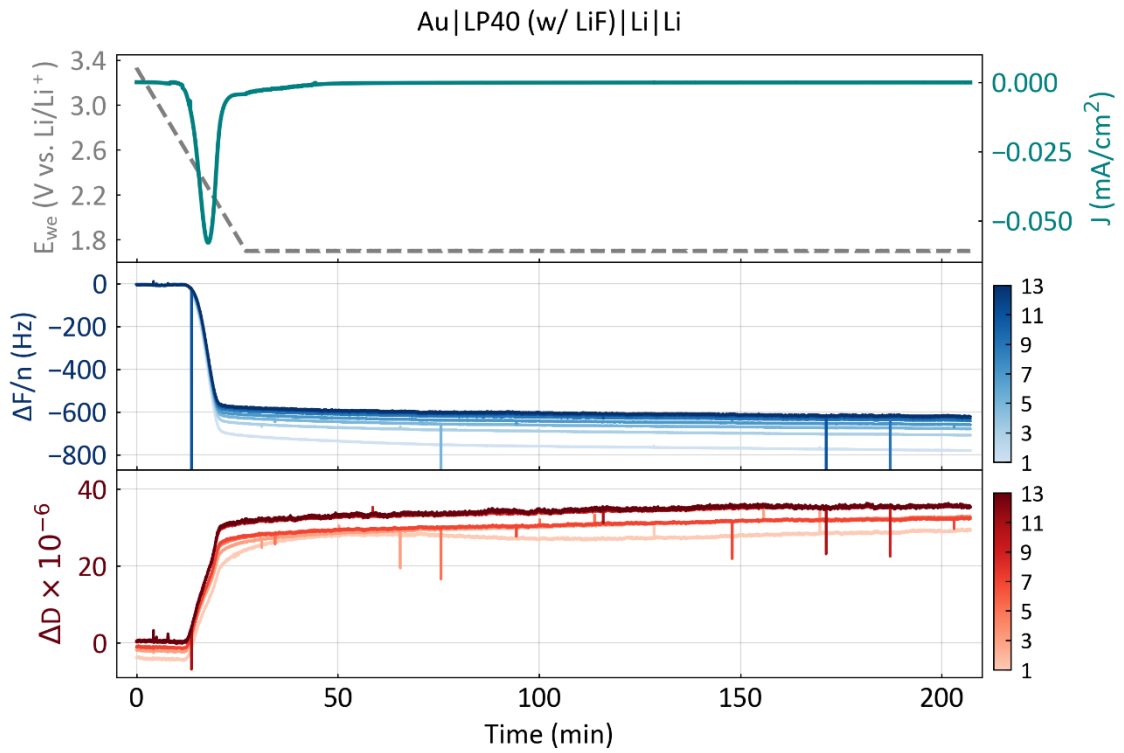

Figure 9 EQCM-D response during LiF-SEI formation on Au. From top to bottom: time-dependent working electrode potential (left) and current density (right); normalized frequency shifts (ΔF/n) for different overtones; and dissipation shifts (ΔD) for different overtones.

Taken together, the raw EQCM-D data show that, although the same electrochemical protocol was applied, the LiF-SEI formation process differs substantially between Pt and Au. A more quantitative comparison was made by estimating the interphase thickness in three different ways: from the cumulative charge passed during formation, from the Sauerbrey-based apparent mass change, and from Voigt-model-based fitting. Since these approaches rely on different assumptions, identical absolute values are not expected. Their main value here lies in comparing the LiF-SEI formed on Pt and Au. The cumulative charge passed during the formation step was used to estimate the LiF-SEI thickness according to Equation (2). This calculation assumes that the full measured charge originates from HF reduction and is completely converted into LiF-SEI growth. It also assumes a dense and homogeneous interphase, so that the molar mass and bulk density of LiF can be used directly in the thickness calculation.

$$d(\mathrm{cm}) = \rho_{\mathrm{LiF}}(\mathrm{C/cm^2})\frac{m_{\mathrm{LiF}}(g/mol)}{\rho_{\mathrm{LiF}}^{\mathrm{mass}}(\mathrm{g/cm^3}) \times zF} \quad (2)$$

The Sauerbrey equation (as shown in Equation (3)) is the most common way to convert EQCM-D frequency shifts into mass changes. Its strict validity is limited to thin, rigid, homogeneous, and evenly distributed films with negligible dissipation. This requirement is approached more closely for Au, while the Pt data deviate clearly from it because of the strong overtone dispersion and large dissipation response. In the present evaluation, the normalized frequency shift of the 5th overtone was used as a representative value. The calculated mass change was converted into an apparent LiF-SEI thickness by assuming a dense and homogeneous LiF layer. The corresponding volume was obtained using the bulk density of LiF and then divided by the geometric area of the WE.

$$\Delta f = -\frac{2{f_0}^2}{A\sqrt{\rho_q \mu_q}}\Delta m = -C\Delta m \quad (3)$$

In Voigt model, the interphase is described as a viscoelastic layer, and this approach is better suited to films that are soft, liquid-coupled, or structurally complex, and is therefore especially relevant for the Pt case. The fitting was carried out using literature-based parameters and physically reasonable approximations for density and viscosity. Figure 10 compares the LiF-SEI thickness estimates obtained from different methods. The interphase formed on Pt is thicker than that formed on Au. On Au, the estimated thicknesses are 24.3 nm from the charge-based calculation, 45.4 nm from the Sauerbrey evaluation, and 46.5 ± 1.8 nm from the Voigt fitting. On Pt, the corresponding values increase to 58 nm, 103 nm, and 81.7 ± 12.1 nm. The lower thickness values obtained from the charge-based calculation, compared with the EQCM-based estimates, suggest that the formed interphase is not well described as a dense and homogeneous LiF layer. Instead, the larger apparent thickness derived from EQCM-D is consistent with a structurally more complex interphase, potentially involving porosity, liquid coupling, or additional non-LiF contributions. The relation between the two EQCM-based estimates also differs clearly between the two substrates. On Au, the Sauerbrey- and Voigt-based values remain close to each other, which is consistent with the relatively small overtone dispersion and lower dissipation observed in the raw EQCM-D data. On Pt, the difference becomes much larger. This agrees with the pronounced harmonic dispersion and the strong dissipation response observed during formation, indicating that the interphase formed on Pt is less adequately described by a simple thin rigid-film approximation. In this sense, the thickness comparison further supports the conclusion that the LiF-SEI formed on Pt and Au differs not only in apparent thickness, but also in mechanical character.

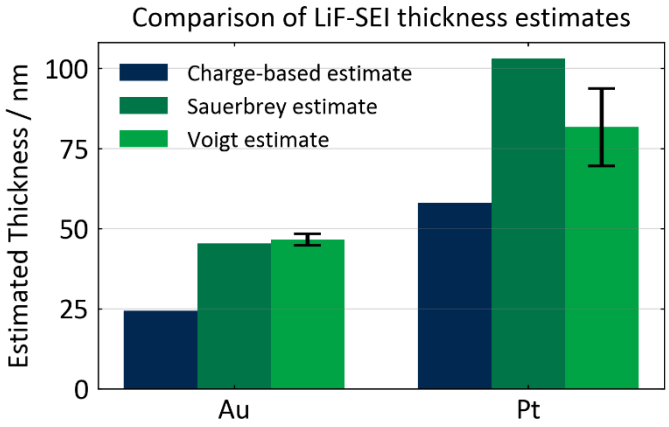

Figure 10 Comparison of LiF-SEI thickness estimates obtained for Au and Pt using different approaches, including the charge-based estimate, the Sauerbrey-based apparent thickness, and the Voigt-model-based thickness.

Scanning electron microscopy (SEM) images recorded after the LiF-SEI formation protocol (Figure 11) reveal clear morphological differences between the interphases formed on Au and Pt. The Au surface is covered by a relatively homogeneous layer consisting of densely packed LiF granular features. In contrast, the Pt surface shows a much more heterogeneous morphology, with large island-like LiF aggregates superimposed on a finer particulate background. This is consistent with a more localized and less uniform interphase formation on Pt, whereas the Au surface appears to be covered more evenly. These morphological differences agree well with the EQCM-D results, which likewise indicate that the LiF-SEI formed on Pt and Au is not identical in structure and growth behaviour.

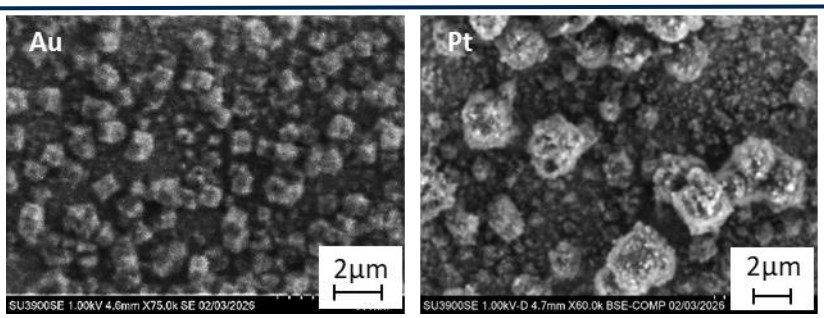

Figure 11 Scanning electron micrographs of the Au (left) and Pt (right) surfaces recorded after the LiF-SEI formation protocol.

3.3 Fc/Fc⁺ redox response after interphase formation

Figure 12 and Figure 13 show the Fc/Fc⁺ redox response recorded after LiF-SEI formation on Pt and Au, respectively. The Fc/Fc⁺ response after LiF-SEI formation showed a clear difference between Pt and Au. On Pt, the oxidation peak current was suppressed at the beginning of the experiment compared with the reference response of the pristine electrode. With continued cycling, however, the current increased steadily and reached about 75% of the reference value within 30 min. The blocking effect of the LiF-SEI on Pt therefore weakened noticeably during repeated scanning. Only one of the three parallel samples (see Figure 12, Sample 2) showed an initial tendency towards a sigmoidal voltammetric response, which may indicate the temporary presence of a porous or locally heterogeneous interphase in that case. On Au, the behavior was considerably more stable, and also much more strongly suppressed. In all three parallel samples, the currents remained low over the entire measurement, and no well-defined redox peak pair was observed. The LiF-SEI formed on Au therefore appears to maintain its blocking character much more effectively under Fc probing conditions than the LiF-SEI formed on Pt. These results already suggest that the LiF-SEI formed on Pt and Au not only differs in its formation behavior, but also in its stability and electron-blocking character during Fc probing.

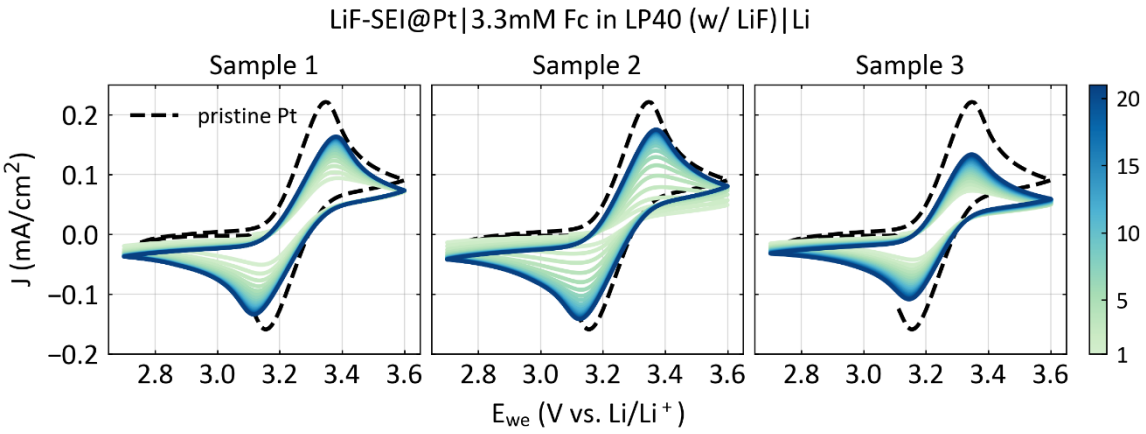

Figure 12 Cyclic voltammograms of the Fc/Fc⁺ redox response recorded on Pt after LiF-SEI formation. The data show three parallel samples measured under identical conditions.

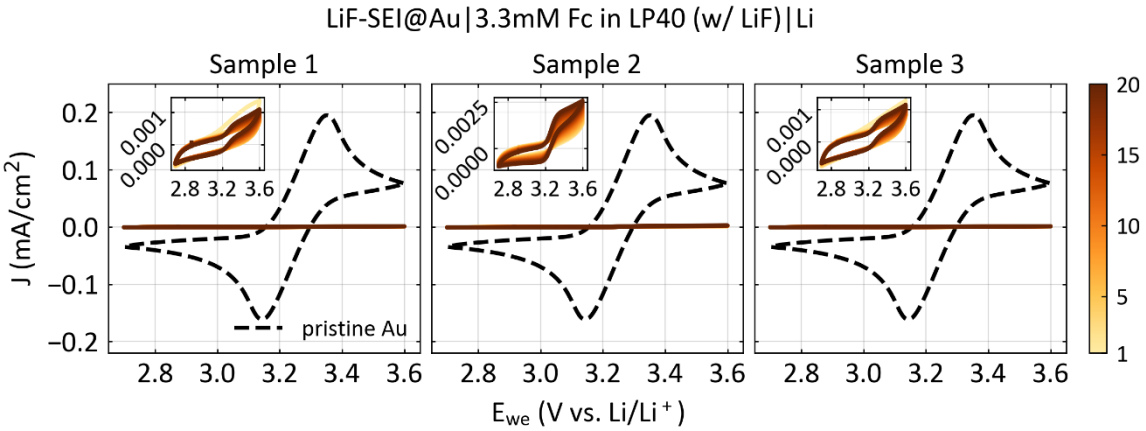

Figure 13 Cyclic voltammograms of the Fc/Fc⁺ redox response recorded on Au after LiF-SEI formation. The data show three parallel samples measured under identical conditions.

Because the Fc/Fc$^+$ response on Pt changed progressively during repeated cycling, complementary EQCM-D measurements were carried out during Fc probing. On Au, the EQCM-D signal remained close to the background level throughout the experiment. The frequency changes were small, on the order of a few tens of hertz, and no clear periodic modulation associated with the Fc redox process could be resolved. Under these conditions, no clear evidence for pronounced LiF-SEI dissolution was obtained. On Pt, the behavior was more complex. During the initial cycles, the EQCM-D response was still close to the background level, similar to that observed on Au. With continued cycling, however, the different overtones began to separate strongly. The lower overtones shifted towards negative values, whereas the higher overtones shifted in the positive direction. In some of the overtones, weak periodic fluctuations became visible that resemble the Fc-related response observed on pristine electrodes. At the same time, the overall magnitude of the frequency change increased to several hundred hertz. This behavior cannot be reduced to a simple picture of direct LiF-SEI dissolution. Instead, it points to a more complex interfacial evolution on Pt during Fc probing.

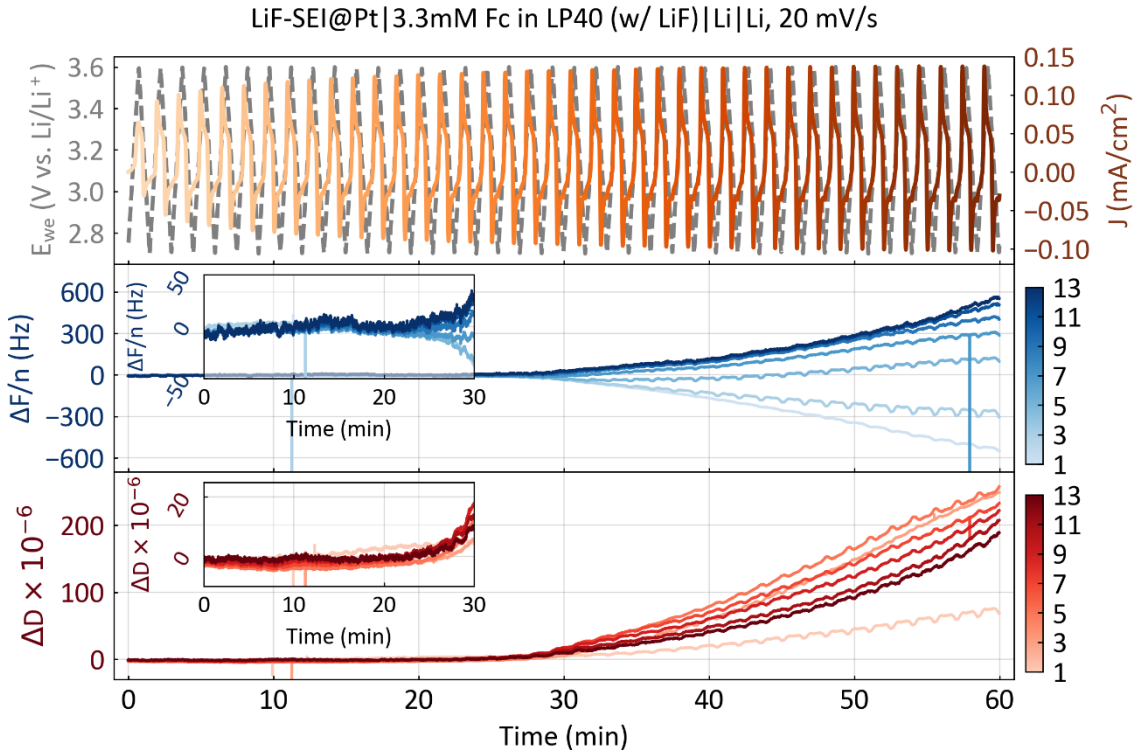

Figure 14 EQCM-D response during Fc redox reactions after LiF-SEI formation on Pt at a scan rate of 20 mV/s. From top to bottom: time-dependent WE potential (left) and current density (right); normalized frequency shifts (ΔF/n) for different overtones; dissipation shifts (ΔD) for different overtones.

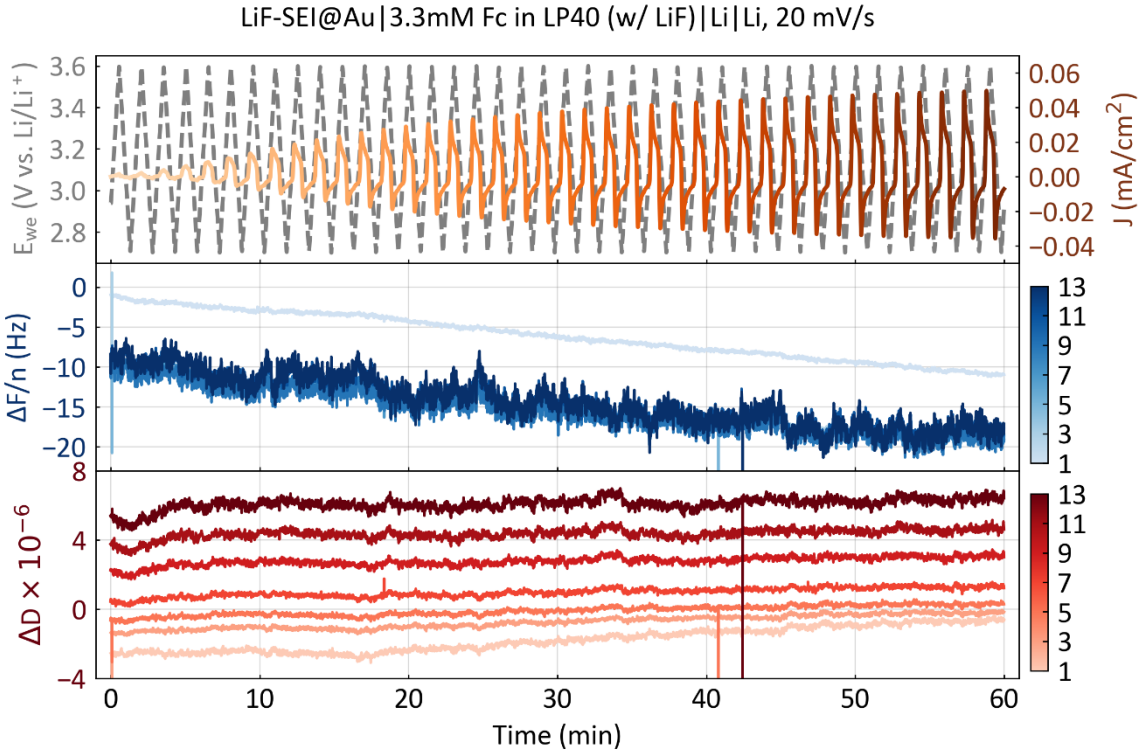

Figure 15 EQCM-D response during Fc redox reactions after LiF-SEI formation on Au at a scan rate of 20 mV/s. From top to bottom: time-dependent WE potential (left) and current density (right); normalized frequency shifts (ΔF/n) for different overtones; dissipation shifts (ΔD) for different overtones.

3.4 Simulation

We perform cyclic voltammetry simulations to interpret the experimental results of the Ferrocene redox shuttle with LiF-SEI. Here, we consider two scenarios: (1) SEI growth via electron tunneling and (2) the effect of a SEI layer with increasing porosity evolution.

First, we consider the effect of electron tunneling on the reaction current. For this scenario, we assume that the reaction forms a passivation layer on top of the working electrode, through which electrons must tunnel to allow for the reaction to continue. This approach is based on a previous simulation study. [4] The simulation of the cyclic voltammogram with tunneling (red) is depicted in Figure 16 in comparison to the one considering the standard case without passivation layer (blue). Without passivation layer, the cyclic voltammogram shows one peak for each voltage sweep, i.e. a peak with negative current for the downward voltage sweep and a peak with positive current for the upward voltage sweep. For the case with electron tunneling, the simulation demonstrates that during the first downward voltage sweep, the reaction begins similarly to the standard case without passivation. However, as the reaction creates a passivation layer the rate reaches a smaller peak value and then decreases again due to the passivation effect. The decrease merges into a current plateau region, where the thickness of the passivation layer increases but the height of the tunneling energy barrier decreases due to the voltage change, leading to a regime with constant current. During the following upward sweep, the height of the energy barrier increases and the tunneling current is blocked completely by the passivation layer. The tunneling also blocks the observed current completely during the following voltage sweeps. Therefore, the cyclic voltammogram with a passivation layer and electron tunneling shows a strongly asymmetric shape during the SEI formation and vanishing current during the following voltage sweeps. This behavior differs from the observed cyclic voltammograms showing non-vanishing currents on Pt and Au electrodes and a rather symmetric shape especially on the Pt electrode.

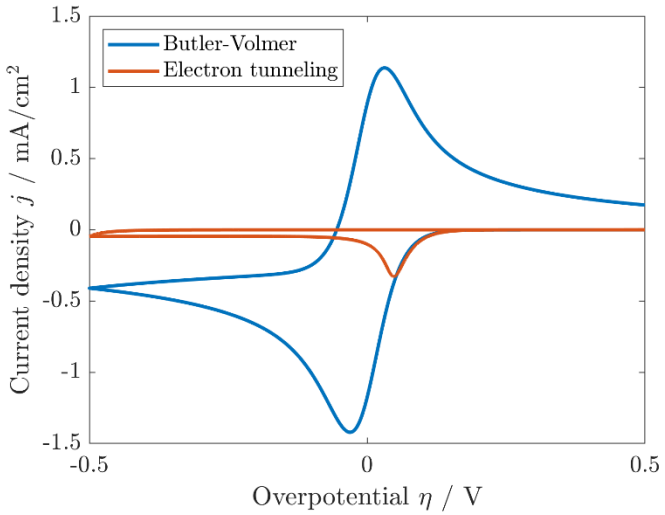

Figure 16 Simulation of cyclic voltammetry with Butler-Volmer reaction rate without passivation (blue) and the reaction rate when the reaction forms a passivation layer through which electrons must tunnel (red).

Next, we consider the influence of a porous SEI layer with increasing porosity over time. This simulation aims to explain the experimental cyclic voltammogram for the Pt electrode in Figure 12, where the current increases over time or with cycle number, respectively. Figure 17shows the simulated cyclic voltammogram with an initially dense SEI and increasing porosity of the SEI over time. Initially, the cyclic voltammogram shows a very small current with only a slight peak during the voltage

sweep (dark blue). The absolute value of the current increases over time and the peaks during the voltage sweep get more pronounced until the end of the simulation (yellow). While the current increases, the position of the peaks remains at the same overpotential value. The increasing currents can be explained by the increasing porosity over time, which leads to an increasing diffusion coefficient of the oxidized and reduced species through the SEI. Comparing the simulation result with the redox experiment on the Pt electrode in Figure 12reveals a good match between the simulation and the experiment. Thus, the evolution of the cyclic voltammogram on the Pt electrode showing increasing currents indicates an increasing porosity of the SEI layer over time according to the simulation. More simulations and experiments are planned to further elucidate this effect or further reasons for the changes in the observed cyclic voltammograms.

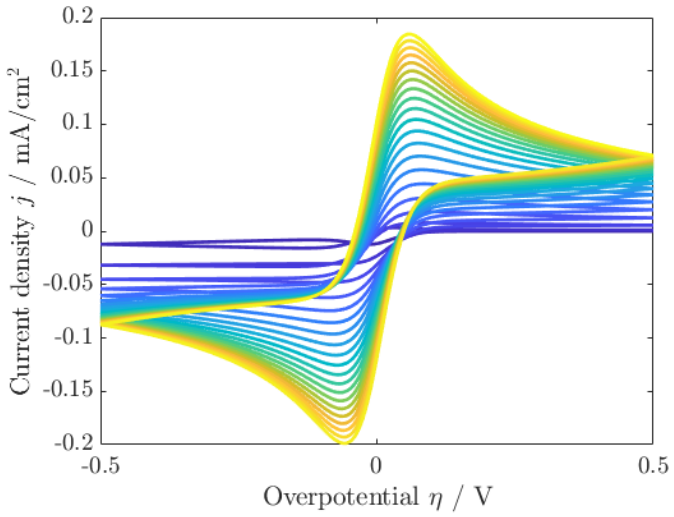

Figure 17 Simulation of cyclic voltammetry with increasing SEI porosity over time (blue = initial cycle, yellow = final cycle)

4 Current Limitations and Remaining Work

The present study focuses on a LiF-based model SEI formed on planar Au and Pt electrodes. This simplified system was deliberately chosen to isolate the effect of a key electronically insulating SEI component and to enable controlled Fc/Fc$^+$ probing of interfacial electron transfer. At the same time, it does not capture the full chemical and structural complexity of SEI formation on practical battery electrodes. The conclusions drawn here should therefore be understood in the context of a model interphase rather than a complete representation of the SEI in realistic electrode systems.

The EQCM-D data obtained during LiF-SEI formation and during Fc probing are highly informative and require further analysis beyond what is possible within the present report. In particular, the Voigt-model evaluation used here is based on a one-layer description of the interphase. The fitting results, however, already suggest that this approximation is not sufficient for Pt, where the interphase behaviour is clearly more complex. We are therefore currently extending the analysis towards hydrodynamic spectroscopy [8] to extract additional information related to porosity, roughness, and other non-rigid interfacial features. The pronounced frequency splitting observed on LiF-SEI-covered Pt during Fc probing is also of particular interest. Its underlying mechanism remains unresolved at present, but it may provide important insight into the dynamic structural evolution of the LiF-SEI under electrochemical perturbation.

The work will continue well beyond the present stage. Ongoing efforts include simulation of the different transport scenarios illustrated in Figure 3, which will be used to generate training data for

machine-learning-based analysis of the experimental Fc redox probe. In parallel, the samples will be investigated by complementary surface and chemical characterization methods such as X-ray photoelectron spectroscopy (XPS), and scanning electron microscopy (SEM). Combining these data with the results obtained from the Fc/Fc^+ redox probe may enable the establishment of a new criterion for assessing SEI quality, namely the passivation efficiency, defined as the ability of the initially formed SEI to suppress further electrolyte decomposition and continued SEI growth. In this way, the method may also provide a route for electrolyte screening. The approach will furthermore be extended beyond the present planar metal model system to more realistic SEI and electrode systems. Current work is already exploring a-Si thin-film anodes, where the Fc/Fc^+ redox probe is being used to quantify passivation efficiency and to compare the passivating behavior of different electrolytes.

5 References

[1] Wang, A., et al., *Review on modeling of the anode solid electrolyte interphase (SEI) for lithium-ion batteries.* npj Computational Materials, 2018. **4**(1): p. 15.

[2] Horstmann, B., F. Single, and A. Latz, *Review on multi-scale models of solid-electrolyte interphase formation.* Current Opinion in Electrochemistry, 2019. **13**: p. 61-69.

[3] Rogers, E.I., et al., *Voltammetric Characterization of the Ferrocene|Ferrocenium and Cobaltocenium|Cobaltocene Redox Couples in RTILs.* The Journal of Physical Chemistry C, 2008. **112**(7): p. 2729-2735.

[4] Steinrück, H.-G., *Modeling cyclic voltammetry during solid electrolyte interphase formation: Baseline scenario of a dynamically evolving tunneling barrier resulting from a homogeneous single-phase insulating film.* The Journal of Chemical Physics, 2021. **154**(17).

[5] Lavacchi, A., et al., *Cyclic voltammetry simulation at microelectrode arrays with COMSOL Multiphysics®.* Journal of Applied Electrochemistry, 2009. **39**(11): p. 2159-2163.

[6] Ge, X., et al., *Electrochemical Removal of HF from Carbonate-based LiPF6-containing Li-ion Battery Electrolytes.* Journal of The Electrochemical Society, 2024. **171**(3): p. 030522.

[7] Strmcnik, D., et al., *Electrocatalytic transformation of HF impurity to H2 and LiF in lithium-ion batteries.* Nature Catalysis, 2018. **1**(4): p. 255-262.

[8] Levi, M.D., et al., *In Situ Porous Structure Characterization of Electrodes for Energy Storage and Conversion by EQCM-D: a Review.* Electrochimica Acta, 2017. **232**: p. 271-284.